ILASS 2008
Sep. 8-10, 2008, Como Lake, Italy

Paper ID ILASS08-1-7

HIGH-SPEED VISUALISATION OF LIQUID JET DISINTEGRATION

Grazia Lamanna*, Ingo Stotz*, Bernhard Weigand*, Johan Steelant°

*Institut für Thermodynamik der Luft- und Raumfahrt (ITLR), Universität Stuttgart
Pfaffenwaldring 31, D-70569 Stuttgart, Germany
°Propulsion and Aerothermodynamics Division (TEC-MPA), ESTEC-ESA
Keplerlaan 1, P.O. Box 299, 2200 AG Noordwijk, The Netherlands
corresponding author: e-mail: grazia.lamanna@itlr.uni-stuttgart.de

ABSTRACT

High-speed shadowgraphy was applied to visualise hydrocarbon spray atomisation at elevated pressures and temperatures. The experiments were performed in the quiescent post-shock region of a double-diaphragm shock tube facility using a heated, fast-response injection system. Test times were in the order of 4.5 ms with reflected-shock pressures ranging from 10-35 bar and test temperatures of 950 K. The fuel (n-hexane and n-dodecane) was injected right after shock reflection and quasi-steady injection was achieved and sustained for about 2.5 ms. Fuel temperature covered both sub- and supercritical values as it was varied between 373.15 and 523.15 K. The acquired images were analysed with respect to the spatiotemporal evolution of the spray, specifically spreading angles and penetration lengths were derived. The influence of the chamber pressure and the fuel temperature on the spray break-up process was investigated. Increasing chamber pressures (chamber densities) and fuel temperatures result in an enhancement of the spray dispersion measured in terms of jet angles and therefore in a better mixing and vaporisation. As one of the two properties (fuel temperature or chamber pressure) is supercritical, incompressible variable-density gas jet behaviour was observed as certain (subcritical) values for the corresponding other one were exceeded.

1 INTRODUCTION

Understanding the injection, break-up, mixing and combustion processes of fuel sprays is of high importance with respect to many propulsion systems, such as rocket, jet, (sc)ramjets and direct injection engines. In this study, a shock tube is used to provide basic information on the injection and disintegration processes of hydrocarbon fuel (e.g. n-dodecane, n-hexane) sprays at elevated fuel and ambient temperatures and pressures. The experiments comprise both (conventional) subcritical fuel disintegration as well as supercritical break-up and are aimed at providing a thorough characterisation of the spray properties as a function of the thermodynamic state.

The disintegration of (liquid) jets has been ascribed to many concurring effects, such as surface tension, viscous and aerodynamic forces, liquid turbulence, cavitation phenomena and liquid supply pressure oscillations. Depending on the break-up mode, the above mentioned interacting factors contribute to the disintegration process with different degree of importance. Extensive reviews on the subject can be found in Lefebvre (1989), Reitz (1978) and Mayer and Telaar (2002). The jet break-up process can be divided into two macroscopic zones, the primary and the secondary break-up region. The primary jet break-up mode can be furthermore classified into different regimes (see Figure 1 for details) depending on the injection pressure, velocity and chamber conditions.

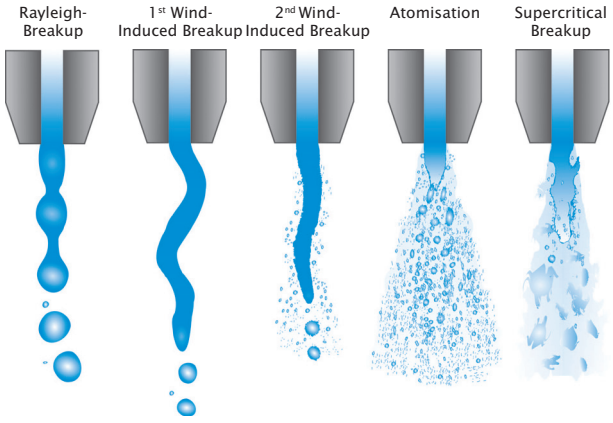

Figure 1. Jet disintegration regimes.

A complete theoretical description of the disintegration process is not yet available. An empirical classification of jet disintegration at atmospheric pressure was given by v. Ohnesorge (1936) using dimensional analysis. The empirical transitions between the different regimes of jet disintegration (Rayleigh breakup, wind-induced breakup and atomisation) can be described as a function of Ohnesorge number versus Reynolds number. More recently, Mayer and Telaar (2002) have extended this empirical classification and included the supercritical breakup. This classifi-

cation, strictly valid only at atmospheric pressures, takes into account the influence of surface tension, viscous, and inertia forces on the disintegration process. With increasing chamber pressures (and therefore chamber densities), these empirical boundaries are shifted towards regions at lower Reynolds numbers. This means that the inception of wind-induced breakup and atomisation occurs at lower outlet velocities compared to atmospheric conditions. At higher chamber densities, the influence of aerodynamics forces and shear stresses on the jet disintegration process increases significantly. Lefebvre (1989) showed that the relevance of aerodynamic forces is well represented by the gaseous Weber number, which consists of the ratio of the disruptive aerodynamic forces and surface tension forces. The increased relevance of the shear stress in a pressurised gas can be represented by the ratio of liquid to gas viscosity. Based on these considerations, Czerwonatis and Eggers (2001) were able to extend the empirical classification for jets to high-pressure conditions by introducing a new non-dimensional number, defined as the product among the Ohnesorge number, the Weber number of the gas phase and the liquid/gas viscosity ratio.

Concerning supercritical disintegration, most studies concentrated on the investigation of cryogenic fuels and surrogates see e.g. (Mayer and Telaar, 2002) and (Chehroudi et al., 2002). In recent reviews, Chehroudi et al. (2003) and Oschwald et al. (2006) analysed in depth the difference between subcritical and supercritical breakup in cryogenic fuels. They were able to identify the mechanism of transition from the wind-induced to the supercritical regime where the jet structure began to resemble a turbulent gas jet with no detectable droplets. The similarity between supercritical and turbulent gas jets was demonstrated by showing that the experimental jet growth rate agreed well with the theory of incompressible, variable density gaseous mixing layers.

The present study focuses on the disintegration of hydrocarbon fuels, especially on the transition from the atomisation to the supercritical regime. In the atomisation regime, both aerodynamic forces and shear stresses play a dominant role in controlling the lateral spreading of the jet. Therefore, it is not clear whether and to what extent a reduction in surface tension may affect the "classical" atomisation process.

In the present study, the injection and chamber condition are varied in such a way as to perform disintegration experiments at both subcritical, near-critical, and supercritical conditions. The analysis is still at a phenomenological level, since not all jet geometrical parameters have been correlated to the available empirical correlations and/or theoretical predictions in the atomisation regimes. Despite these limitations, clear trends could be identified, as discussed in Section 4.

2 EXPERIMENTAL SETUP

2.1 ITLR Test Facility

The test facility for jet disintegration studies consists of a double-diaphragm shock tube (DDST), equipped with a fast-response, heated injector. Test times of the order of typically $2-5$ ms are attainable with reflected-shock pressures up to 50 bar and typical temperatures of up to 2000 K. A more detailed description and qualification of the facility is provided in Stotz et al. (2008). Figure 2 provides a schematic view of shock tube. The (square) test chamber is equipped with flat flush-mounted fused-silica windows on both side walls, which cover the full height of the duct over a length of 60 mm. The fast-response heated injector is flush-mounted in the end flange in a way that fuel is injected perpendicularly to the endwall into the gas behind the reflected shock wave. Fuel pressures can be varied between ≈ 100 and 1400 bar, fuel temperatures as high as 573.15 K can be achieved with the present system.

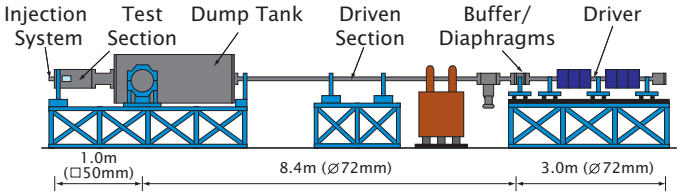

Figure 2. Schematic drawing of the ITLR double-diaphragm shock tube.

2.2 Optical Setup

The optical layout of the shadowgraph setup is shown in Figure 3. A collimated beam,emitted by a high-power LED lamp (Luxeon Rebel) and slightly larger than the test-section's window diagonal, back-illuminates the spray. The light is subsequently collected by a parabolic mirror ($f = 900$ mm, $D = 150$ mm) and focused on the CMOS chip of the camera by a Schneider-Kreuznach Super-Symmar HM 5.6/150 objective lens. The optical setup results in a magnification factor of $MF = 1{:}6$, which corresponds to an effective optical resolution of about 120 μm and yields a maximum theoretical velocity without motion blur of $v = 120$ m/s. The high-speed camera used is a Photron Fastcam SA1. High-speed images were recorded at a resolution of 512x96 pixels and 512x160 pixels at acquisition frame rates of 100,000 fps and 62,500 fps, respectively.

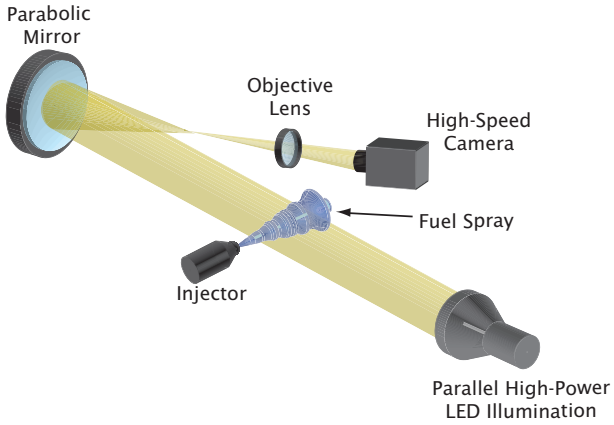

Figure 3. Optical setup for the high-speed imaging experiments.

3 DATA REDUCTION

3.1 Postprocessing

The extraction of accurate spray geometrical data from the shadowgraph images requires image processing that reduces background noise and enhances the image contrast

without altering the spray contour.

Illumination inhomogeneities due to temporal fluctuations as well as spatial non-uniformities of the light distribution are accounted for by normalising each image to a reference image, thus the background intensity of all images of an experimental series is homogenously distributed and at a constant value. Afterwards, the images are filtered with a (two-dimensional) hybrid, edge-preserving median filter to reduces the background noise, caused by the shock tube flow, without influencing the shape of the spray.

Subsequently, the spray images are thresholded to separate the spray from the background. Unfortunately, the contour of an atomising and evaporating spray is not clearly confined, as it is made up, especially in the outer region, of a mixture of liquid fuel, ambient test gas, fuel vapour and, depending on the test conditions, supercritical fluid. On this account, the results may depend on the level on which the spray images are thresholded, as the spray contour marks the smooth transition between the spray and the ambient test gas. For this purpose, a sensitivity analysis was performed. For threshold levels between 40 and 70 % of the background intensity, the deviations in the spray angles are usually smaller than 1 deg. All tests reported in the following sections, are evaluated using a 50% threshold, which represents an intermediate value among those physically reasonable.

Additionally, subpixel interpolation is applied to increase the spatial resolution of the images, which enhances the accuracy of the analysis. This improvement in accuracy is particularly relevant for the region closer to the nozzle, where a shift of the spray contour by a single pixel may cause high deviations from the "real" value. As an example for the resulting images, Figure 4 shows the temporal evolution of an n-hexane spray injected at a chamber pressure of $p_5 = 35\,\text{bar}$ and a fuel temperature of $T_f = 523.15\,\text{K}$.

3.2 Definition of the Jet Parameters

In the evaluation of the spray characteristics, the following macroscopic parameters will be considered: (local) jet spreading angle, spray tip length and velocity (in the start up phase) and dark (dense) core length. Their geometrical definition is illustrated in the bottom image of Figure 4. In the present work, the axial distribution of the local spreading angle $\theta_i(x)$ is considered, as it provides a better physical insight in the spatiotemporal evolution of the (fuel) spray and its interaction with the surrounding test gas. The spreading angle is directly related to the rate of gas entrainment into the jet and is influenced by the forces acting on the jet at the nozzle exit. Depending on the chamber and injection conditions, the local spreading angle may vary along the axis, as shown in Figure 5. The picture shown here is the average image, composed of 150 single snapshots (during "quasi-steady" injection) of a single experiment. For a more accurate description of the lateral spreading of the spray and to facilitate the comparison among literature data, it is therefore advisable to investigate the axial distribution of the local spray angle $\theta(x)$.

In literature, two different characteristic lengths are often employed to describe the axial penetration of the spray: the spray tip length L_{spray} and the dense core length L_{core}. The spray tip penetration (axial growth rate) is calculated from the extent of the spray contour during the start-up process of the injection. Using the spray lengths of all

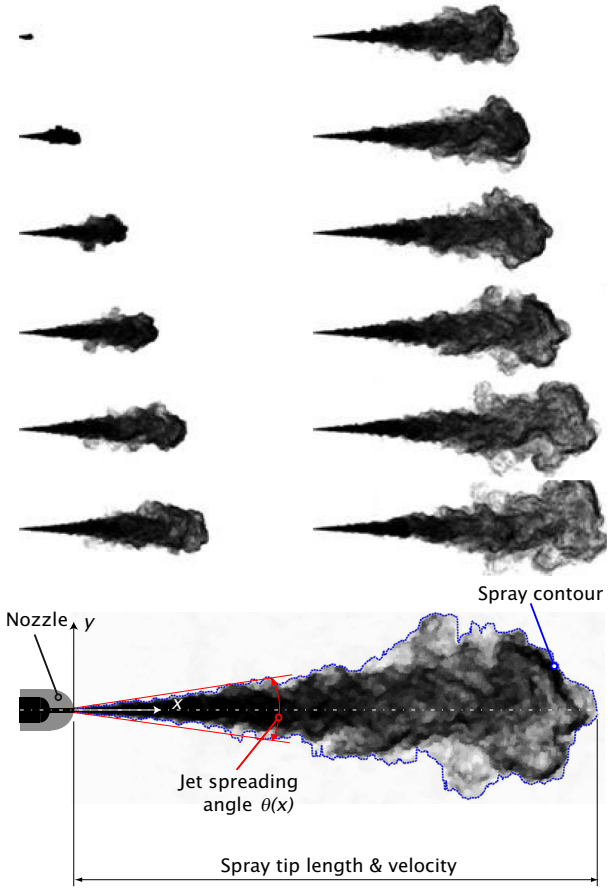

Figure 4. Example of a series of spray shadowgraph images (time between images $\Delta t = 160\,\mu\text{s}$) and definition of jet parameters.

images and the chosen frame rate of the camera, the (transient) velocity of the spray tip v_{spray} can be derived.

The liquid or dense core length of the jet is a measure for the axial penetration of the jet/spray core into the test environment. The "liquid core" can be either specified as the intact core (connected liquid) or as the dense core (high liquid/gas density ratio). The dense core length is calculated in a similar manner as the spray tip length, albeit with a much smaller threshold (2% of the background intensity level), in order to include only the dense (i.e. dark, low-intensity) parts of the spray. Although this quantity is rather arbitrary and also dependent on the threshold level chosen, it is still a useful measure to compare different conditions among each other, to classify break-up processes and to identify steady state injection conditions, provided the threshold level is consistent through the analysis.

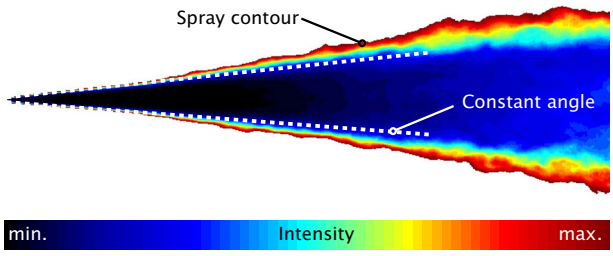

Figure 5. Average image of the spray.

4 RESULTS

4.1 Test conditions

The experiments were performed in the region behind the reflected shock wave. The test pressure p_5 was varied between 10 and 35 bar while the test temperature was fixed at a target value of $T_5 = 950\,\mathrm{K}$. The fuel back-pressure was set so as to maintain a constant pressure difference between fuel reservoir and test chamber of $\Delta p_f = p_f - p_5 = 200\,\mathrm{bar}$. As the effect of fuel preheating was to be investigated, three different fuel temperatures were selected: $T_f = 373.15$, 448.15 and 523.15 K. The test conditions of the present study are summarised in Table 1.

Condition No.	p_5 [bar]	T_5 [K]	ρ_5 [kg/m^3]
I	10.0 ± 0.05	952 ± 6	5.1 ± 0.04
II	27.5 ± 0.04	951 ± 5	13.6 ± 0.09
III	35.0 ± 0.16	949 ± 8	17.5 ± 0.14

Table 1. Chamber conditions of the experiments performed in the present study. Test pressures, temperatures and densities were derived from the incident shock Mach number M_s. The uncertainties quoted are the standard deviations of different experiments.

Two fuels n-dodecane and n-hexane were tested using a nozzle with a rounded inlet, an inner diameter of $D = 236\,\mu\mathrm{m}$ and a length to diameter ratio of $L/D = 4$. In order to thermodynamically characterise the experimental conditions, the reduced temperature and pressure are introduced. They are defined as the ratio of the actual to the critical fuel temperature ($T_r = T_f/T_c$), the ratio of the chamber pressure to the critical fuel pressure ($p_r = p_5/p_c$) respectively. In the case of n-dodecane, p_r varies in the range $0.55 \leq p_r \leq 1.91$, while T_r lies between ($0.57 \leq T_r \leq 0.79$). For n-hexane, the reduced temperature varies in the range of $0.73 \leq T_r \leq 1.03$ and the reduced pressure between $0.33 \leq p_r \leq 1.15$. The most significant difference between the two experimental campaigns is that, for n-hexane, an excursion above the critical point is possible both in temperature and pressure, while for n-dodecane the initial fuel temperature is below its critical value.

4.2 Results for n-Dodecane

The influence of the chamber pressure p_5 (density ρ_5) on the spray dispersion and penetration is shown in Figure 6. As a first remark, note that the results for $p_5 = 27.5\,\mathrm{bar}$ and $p_5 = 35\,\mathrm{bar}$ are generally very similar, whereas those for $p_5 = 10\,\mathrm{bar}$ differ considerably. In terms of reduced thermodynamic parameters, this means that as soon as $T_r \geq 0.79$ and $p_r \geq 1.50$, subcritical jet disintegration starts to deviate from "standard" atomisation. The term "standard" atomisation refers to the fact that spreading angle increases with an increase in chamber density. This represents an established trend for the atomisation regime, in agreement with the experimental observations of e.g. Hiroyasu and Arai (1990), Naber and Siebers (1996), Chehroudi et al. (1985). The most striking difference is traceable in axial distribution of the time averaged ($t = 2 - 4.5\,\mathrm{ms}$) jet spreading angle, shown in Figure 6(a)-6(b). For a reduced pressure much smaller than one ($p_r \approx 0.5$), the spray angle is almost constant for the whole observable distance and only a very faint increase is found. As the reduced parameters are increased, but still remaining in the subcritical region (i.e., $p_r \geq 1.5$ and $0.68 \leq T_r \leq 1$), the jet disintegration can be divided in two distinct zones. In the near-nozzle region (up to about $x/D \approx 40$), fairly constant angles are observed. In the downstream region, the spray angles increase with a nearly linear slope. As a general trend, higher pressures and densities lead to larger spray angles at all axial positions. The position at which the curves start to diverge coincides approximately with the onset of the breakup region at $t = t_0$ (breakup time, following the terminology of Hiroyasu and Arai (1990)). For $t > t_0$ the spray is slowed down and the influence of higher chamber pressure becomes more relevant through the enhanced gas entrainment. This region, further downstream of the nozzle tip, is dominated by turbulent shear-layer mixing effects.

Concerning the region near the nozzle tip, "standard" atomisation is observed for $p_r = 0.55$ and $T_r \leq 0.68$. However, at supercritical chamber pressures and higher (but subcritical) reduced temperatures ($T_r \geq 0.79$), the jet angles appear to diverge from the density dependence observed at lower pressures. As can be clearly seen in Figure 6(b), the spray angle (near the nozzle tip) hardly changes as the chamber pressure is increased from 27.5 to 35 bar. Furthermore, as the reduced temperature is increased to ≈ 0.8 (i.e. $T_f = 523.23\,\mathrm{K}$), the spreading angle approaches the lower limit of incompressible, fully developed jets (i.e. $tan(\theta) \approx 0.2$), already at values of the ambient-gas to fuel density ratio of the order of 0.02 (i.e. $\rho_{ch}/\rho_f \approx 0.02 - 0.03$). A similar behaviour was also found experimentally by Chehroudi et al. (2002) for the transition from the second-wind induced breakup regime and marked as the onset of supercritical disintegration. Note that for atomisation experiments performed at much lower reduced temperatures ($T_r \approx 0.4$), the transition towards incompressible jet behaviour is predicted for much larger density ratios ((i.e. $\rho_{ch}/\rho_f \approx 1$) (see e.g. Naber and Siebers (1996)). This seems to suggest that, in the near-nozzle region, the spray disintegration in the subcritical regime start to resembles more and more that of an incompressible jet, as soon as the injection/chamber conditions approach the critical values of the injectant.

The spray tip length during the first phase of fuel injection is given in Figure 6(c). During the first $300 - 400\,\mu\mathrm{s}$, the penetration and thus the velocity of the spray tip is very similar for all three pressures investigated. At this point, the spray tip gets noticeably decelerated for the two higher pressures, while it remains on a fairly constant velocity for the lower pressures 10 bar. After about $800\,\mu\mathrm{s}$, an observable difference is also found for 27.5 and 35 bar. Spray tip velocities can thus be assumed to be constant in the initial stage of jet propagation (inertia-dominated). After a certain time t_0, to which Hiroyasu and Arai (1990) refer to as the break-up time of the spray, the spray is remarkably slowed down. This deceleration is stronger for higher chamber pressure (density) and occurs noticeable earlier as the resistance of the gas is higher the denser it gets. The spray tip penetration, as well as the time of the transition between the linear behaviour and the attenuated growth, decreases with increasing chamber pressure.

During this deceleration phase, the spray penetration is attenuated and follows a power function of the form $L_{spray} \sim t^c$ ($c < 1$). The spray tip velocities v_{spray}, derived from the temporal evolution of tip lengths, are all smaller than 90 m/s, which is significantly smaller than

the calculated ideal theoretical velocity $v_{theo} \approx 230\,\mathrm{m/s}$ for a differential pressure $\Delta p = 200\,\mathrm{bar}$ at the orifice outlet. This leads to the conclusion that the spray disintegration already starts shortly after or directly at the nozzle outlet.

As can be seen in Figures 6(d) and 6(e) the dark core length L_{core}, indicated by the 2%-intensity contour of the spray, reflects similar behaviour at the beginning of the injection as the spray tip length. After about 1 ms, it then abruptly comes to rest and stays constant for the rest of the test time. As an effect of the reduced aerodynamic resistance, these (constant) values are larger for smaller chamber densities. For the highest temperature, the discrepancies of the dark core penetration vanish and, for all chamber pressures (densities), virtually equal lengths are found.

In addition to the chamber pressure, the influence of the fuel temperature was investigated. Its influence on the local spreading angle is shown in Figures 7(a) and 7(b). As can be seen, the fuel temperature has only a marginal influence on the jet spreading angle. For low reduced pressures ($p_r = 0.5$, i.e. $p_5 = 10\,\mathrm{bar}$), differences are observed in the upstream region close to the nozzle, which follows the "classical" atomisation behaviour. It is not surprising that the fuel temperature has only an indirect impact on the jet spreading angle. In fact, the fuel temperature affects indirectly the ambient-gas to fuel density ratio by reducing the fuel density. This circumstance implies slightly larger spreading angles for increasing fuel temperatures, as confirmed by a visual inspection of Figure 7(a). At high reduced pressures ($p_r = 1.9$, i.e. $p_5 = 35\,\mathrm{bar}$) and for $T_r \geq 0.68$ ($T_f \geq 448.15\,\mathrm{K}$), the fuel temperature has practically no impact at all on the lateral spreading of the jet. In fact, at these reduced thermodynamic parameters, the spray behaviour (in the near-nozzle region) evolves towards the behaviour of an incompressible jet and therefore it is completely insensitive to variations in the ambient-gas to fuel density ratio. Concerning the region further downstream of the nozzle, aerodynamic forces and turbulent mixing dominate the lateral spreading of the jet. This explains the convergence towards a similar value regardless of the specific value of the fuel injection temperature.

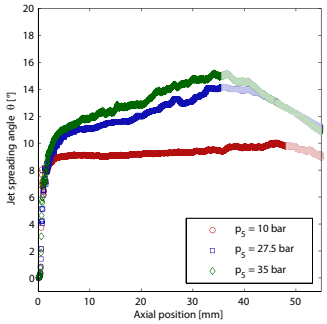

(a) Time averaged spreading angle θ versus axial distance, T_f=448.15 K

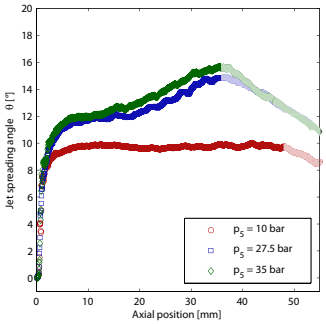

(b) Time averaged spreading angle θ versus axial distance, T_f=523.15 K

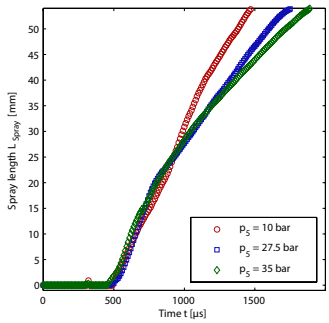

(c) Spray tip length L_{spray} versus time, T_f=448.15 K

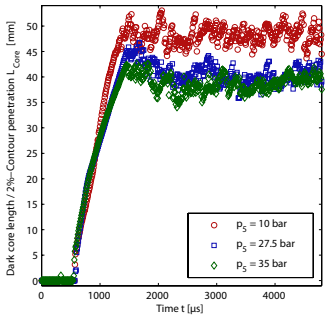

(d) Dark core length L_{core} versus time, T_f=448.15 K

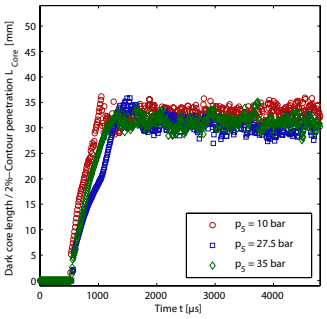

(e) Dark core length L_{core} versus time, T_f=523.15 K

Figure 6. Influence of the chamber pressure on the jet spreading angle θ, the spray tip length L_{spray} and the dark core length L_{core} (fuel: n-dodecane).

The spray tip velocity is hardly influenced by the fuel temperature. All spray tip traces develop very similarly and almost collapse to a single curve. This holds for all chamber pressures investigated, i.e. the rate of spray tip propagation L_{spray} is dominated by the resistance due to aerodynamic forces and the kinetic energy of the fuel at the nozzle outlet. As expected the dark core length L_{core} in turn is strongly influenced by the initial jet temperature, as increased temperatures lead to enhanced evaporation and thus to shorter penetration of the dense spray core. Similar behaviour is observed for all chamber pressures.

4.3 Results for n-Hexane

The most significant difference between the two experimental campaigns is that, for n-hexane, an excursion above the critical point is possible both in temperature and pressure as the critical temperature of n-hexane (507.9 K) is noticeably below that of n-dodecane (658.7 K). More specifically, reduced temperatures were varied in the range of $0.73 \leq T_r \leq 1.03$ and reduced pressures between $0.33 \leq p_r \leq 1.15$.

Figure 8 provides an overview of the influence of the chamber gas pressure (density) on the jet break-up process for a subcritical ($T_r = 0.73$) and a supercritical ($T_r = 1.03$) reduced temperature. At subcritical temperatures and low subcritical (see Figure 8(a)) "standard" atomisation behaviour is observed in the near-nozzle region, i.e. the spreading angle increases with increasing chamber densities. In the region further downstream of the nozzle, the lateral spreading of the jet is controlled by turbulent mixing and gas entrainment and, similarly to the n-dodecane experiments, much more sensitive to the chamber density.

Figure 8(b) shows the pressure dependence of the jet spreading angle at a (supercritical) reduced temperature $T_r = 1.03$. As can be seen, the jet lateral spreading in the near-nozzle region is independent of the chamber pressure and tends to the limit of $tan(\theta) \approx 0.2$ already at a reduced (subcritical) pressure of $p_r = 0.91$. As for all other experiments, the downstream region ($x/D \geq 40$) resembles the behaviour of a turbulent mixing layer and the lateral

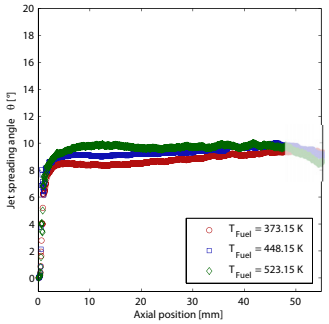

(a) Time averaged spreading angle θ versus axial distance, p_5=10 bar

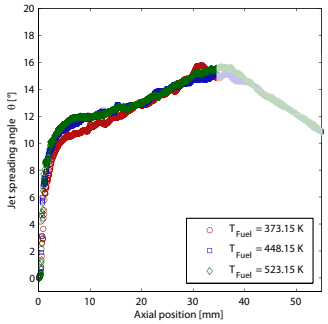

(b) Time averaged spreading angle θ versus axial distance, p_5=35 bar

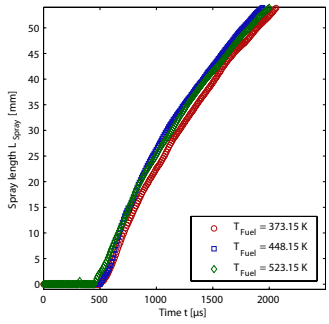

(c) Spray tip length L_{spray} versus time, p_5=35 bar

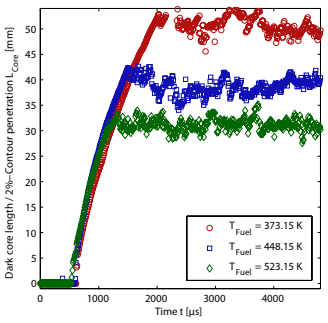

(d) Dark core length L_{core} versus time, p_5=35 bar

Figure 7. Influence of the fuel temperature on the jet spreading angle θ, the spray tip length L_{spray} and the dark core length L_{core} (fuel: n-dodecane).

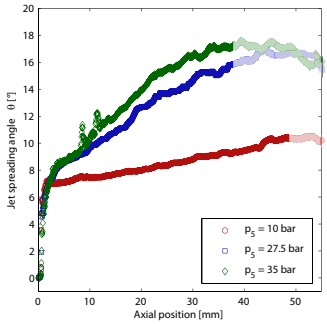

(a) Time averaged spreading angle θ versus axial distance, T_f=373.15 K

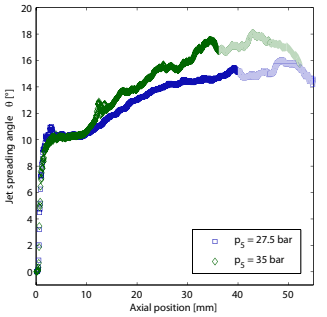

(b) Time averaged spreading angle θ versus axial distance, T_f=523.15 K

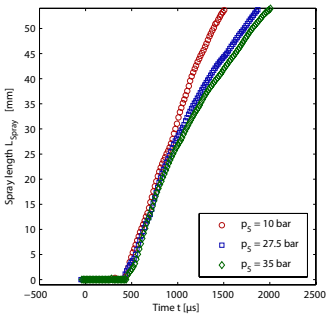

(c) Spray tip length L_{spray} versus time, T_f=373.15 K

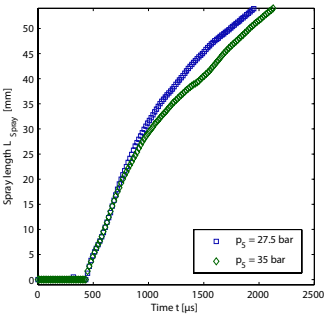

(d) Spray tip length L_{spray} versus time, T_f=523.15 K

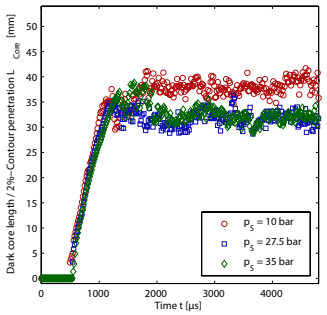

(e) Dark core length L_{core} versus time, T_f=373.15 K

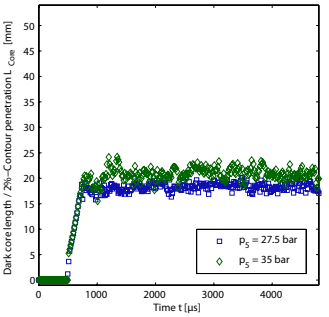

(f) Dark core length L_{core} versus time, T_f=523.15 K

Figure 8. Influence of the chamber pressure on the jet spreading angle θ, the spray tip length L_{spray} and the dark core length L_{core} (fuel: n-heptane).

spreading is a function of the chamber density.

The spray length during the initial phase of the injection process is plotted in Figure 8(d) for the (supercritical) fuel temperature $T_f = 523.15\,\mathrm{K}$ ($T_r = 1.03$). At the very beginning, the penetration and thus the velocity of the jet is virtually equal for all pressures investigated. Thereafter, the tip gets decelerated and the penetration depth is shorter for increasing chamber pressure. Comparing these observations with those for subcritical injection (fuel temperature $T_f = 373.15\,\mathrm{K}$, $T_r = 0.73$) does not show any qualitative differences (see Figure 8(c)). This implies that the propagation of the spray tip is governed solely by inertia and aerodynamic forces.

For n-hexane, the dark core length is only influenced slightly by the chamber pressure and more noticeably for cooler fuel temperatures. For $T_f = 373.15\,\mathrm{K}$ ($T_r = 0.73$) slightly longer dark core lengths are observed for $p_5 = 10\,\mathrm{bar}$ ($p_r = 0.33$)(see Figure 8(e)), whereas for $p_5 = 27.5$ or higher ($p_r \geq 0.91$), the dark core length levels out at a constant value regardless of the chamber pressure value. If the reduced temperature T_r is increased to values > 1 (see Figure 8(f)), no major difference is observed in the dark core lengths. Similarly to the results obtained for n-dodecane, the fuel temperature, rather then the chamber pressure, seems to be the controlling parameter for the dark core length.

For n-hexane, the fuel temperatures were varied from subcritical to supercritical values, as possible differences in the disintegration mode were to be investigated. The influence of the fuel temperature is shown in Figure 9. The axial variation of the jet spreading angle θ is given in Figures 9(a) and 9(b), for subcritical ($p_r = 0.91$) and supercritical ($p_r = 1.15$) reduced pressures. For both reduced pressures, two distinct zones can again be identified (close to the nozzle exit (up to $x/D \approx 40$) and further downstream). In the near nozzle region, the standard atomisation process evolves slowly towards gas jet behaviour, identified by the limit $tan(\theta) \approx 0.2$, as soon as the fuel temperature is increased beyond the critical value $T_r = 1.03$. The downstream zone in turn is quite insensitive to the initial fuel temperature, equal values are found for different fuel temperatures and equal chamber conditions.

No influence on the spray tip length and its velocity was observed for all fuel temperatures for both subcritical (Figure 9(c)) and supercritical (Figure 9(d)) chamber pressures p_5. This also shows that the dominating parameter for spray propagation is the chamber pressure/density, as this provides the resistance to the penetrating jet. Variations in the evaporation rate due to different fuel temperatures only play (if any) a minor role.

The dark core length, in turn, exhibits a strong dependence upon the fuel temperature. In general, an increase in the fuel temperature leads to shorter dark core lengths (see

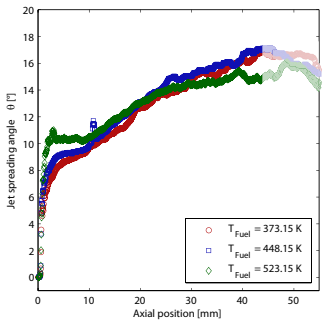

(a) Time averaged spreading angle θ versus axial distance, p_5=27.5 bar

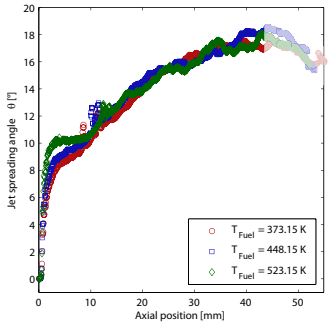

(b) Time averaged spreading angle θ versus axial distance, p_5=35 bar

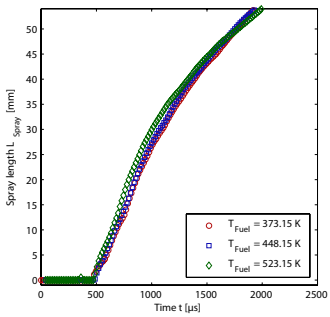

(c) Spray tip length L_{spray} versus time, p_5=27.5 bar

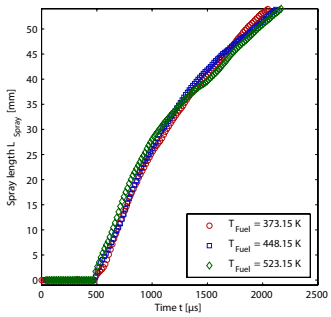

(d) Spray tip length L_{spray} versus time, p_5=35 bar

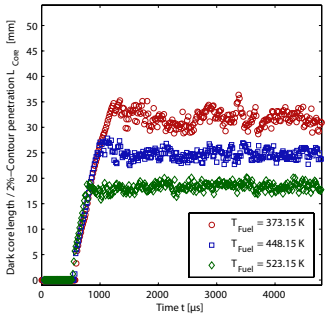

(e) Dark core length L_{core} versus time, p_5=27.5 bar

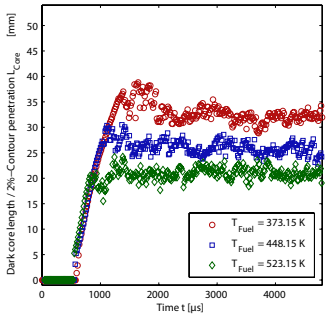

(f) Dark core length L_{core} versus time, p_5=35 bar

Figure 9. Influence of the fuel temperature on the jet spreading angle θ, the spray tip length L_{spray} and the dark core length L_{core} (fuel: n-heptane).

Figure 9(f)), regardless of whether the chamber pressure is below or above the critical value. This can be clearly seen by comparing Figures 9(e) and 9(f).

As a concluding remark, we would like to point out the limitation of the shadowgraph imaging technique of not being capable to distinguish between liquid phase and dense gas. It is therefore not clear whether the similarity between near critical and supercritical conditions can be extended beyond geometrical parameters (e.g. jet spreading angle or dark core length). With reference to Figure 9(f), for example, it is impossible to ascertain whether the inner core of the spray consists of a liquid, dense gas, supercritical fluid or a mixture of all as the reduced temperature is increased from $p_r = 0.73$ to 1.03.

5 CONCLUSION

Hydrocarbon fuel injection experiments have been conducted in a shock tube to experimentally investigate jet disintegration in the subcritical (atomisation) and supercritical regime. The fuel was injected into an inert test gas environment (argon), whose temperature was set to a fixed supercritical temperature while the gas pressure was varied from sub- to supercritical values. The injection and breakup processes were visualised by means of high-speed shadowgraphy. The experiments show that for a reduced pressure much smaller than one, the spray atomises in the "standard" way. As soon as the reduced parameters approach the critical point, the disintegration process can be divided in two distinct zones: specifically, the near nozzle region (up to $x/D \approx 40$) and the downstream region. In the region further downstream of the nozzle, the lateral spreading of the jet is controlled by turbulent mixing and gas entrainment and is therefore much more sensitive to the chamber density. In the near-nozzle region, the experimental results support the hypothesis that the jets behave similar to an incompressible gas jet, provided that one of the two parameters p_r or T_r is larger 1 and the other one is above a specific value $\approx 0.8 - 0.9$. This statement is corroborated by the quantitative agreement of the jet growth rate measurements with those predicted by the theoretical equations for incompressible gaseous jets.

ACKNOWLEDGMENTS

This work was performed within the *Long-Term Advanced Propulsion Concepts and Technologies (LAPCAT)* project investigating high-speed airbreathing propulsion. *LAPCAT*, coordinated by *ESA-ESTEC*, is supported by the *EU* within the 6^{th} *Framework Programme* Priority 1.4, Aeronautic and Space, Contract no.: AST4-CT-2005-012282. Further information on *LAPCAT* can be found on: `http://www.esa.int/techresources/lapcat`.

The authors are also gratefully indebted to the Landesstiftung Baden-Württemberg for facilitating the high-speed experiments entailed in this paper.

References

B. Chehroudi, S. H. Chen, F. V. Bracco, and Y. Onuma. On the Intact Core of Full-Cone Sprays. In *Society of Automotive Engineers Congress and Exposition Transaction Papers*, 1985. Paper No. 850126.

B. Chehroudi, D. Talley, and E. Coy. Visual Characteristics and Initial Growth Rates of Round Cryogenic Jets at Subcritical and Supercritical Pressures. *Physics of Fluids*, 14(2):850–861, February 2002. doi: 10.1063/1.1430735.

B. Chehroudi, D. Talley, W. Mayer, R. Branam, J. Smith, A. Schik, and M. Oschwald. Understanding Injection into High Pressure Supercritical Environments. In 5^{th} *International Conference on Liquid Rocket Propellants*, Chattanooga, USA, October 27–30 2003.

N. Czerwonatis and R. Eggers. Disintegration of Liquid Jets and Drop Drag Coefficients in Pressurized Nitrogen and Carbon Dioxide. *Chem. Eng. Technol.*, 24(6):619–624, 2001.

H. Hiroyasu and M. Arai. Structures of Fuel Sprays in Diesel Engines. Number Doc. No. 900475, 1990.

A. H. Lefebvre. *Atomization and Sprays*. Taylor & Francis Inc., 1989.

W. Mayer and J. Telaar. Investigation of Breakup of Turbulent Cryogenic Variable-Density Jets. *Atomization and Sprays*, 12(5&6):651–666, 2002.

J. D. Naber and D. L. Siebers. Effects of Gas density and Vaporization on Penetration and Dispersion of Diesel Sprays. In *SAE International Congress and Exposition*, number SAE Paper No. 960034, 1996.

M. Oschwald, J. Smith, R. Branam, J. Hussong, A. Schik, B. Chehroudi, and D. Talley. Injection of Fluids into Supercritical Environments. *Combustion Science and Technology*, 178(1-3):49–100, 2006.

R. Reitz. *Atomization and other Breakup Regimes of a Liquid Jet*. PhD thesis, Princeton University, Princeton, NJ, 1978.

I. Stotz, G. Lamanna, B. Weigand, and J. Steelant. Shock Tube Study on Hydrocarbon Free Jets using High-Speed Shadowgraphy. In *Proceedings of the 15th AIAA Space Planes and Hypersonic Systems and Technologies Conference*, number AIAA-2008-2538. AIAA, 28 April – 1 May 2008.

W. v. Ohnesorge. Die Bildung von Tropfen an Düsen und die Auflösung flüssiger Strahlen. *Z. Angew. Math. Mech.*, 16:355–358, 1936.